Voltage-gated sodium channels (VGSCs) play important roles in initiation and propagation of action potentials.[1,2] VGSCs consist of one pore-forming α-subunit and one or two β-subunits.[1,2] The α-subunit is made up of four domains (domains I–IV), each containing a motif of six transmembrane segments (S1–S6). The fourth segment (S4) of each domain is positively charged for voltage sensing.[1,3] The VGSC repertoire in humans includes nine α subunits ($Na_v1.1$–$Na_v1.9$), of which $Na_v1.1$, $Na_v1.2$, and $Na_v1.3$, encoded by *SCN1A*, *SCN2A*, and *SCN3A*, respectively, are highly expressed in the brain[4] and when mutated can cause epilepsy.[3,5]

Na_v 1.6, encoded by *SCN8A*, is a major α-subunit in excitatory neurons of the central and peripheral nervous systems, and concentrates in the soma, axon initial segments, dendrites, and nodes of Ranvier.[2,6–8] Recently, a de novo *SCN8A* mutation, which results in a dramatic increase in persistent sodium current and incomplete channel inactivation, was identified in a patient with an infantile epileptic encephalopathy who died of sudden unexplained death in epilepsy (SUDEP).[9] Other de novo *SCN8A* mutations were found in a patient with intellectual disability and tonic–clonic seizures, and another patient with epileptic encephalopathy,[10–13] suggesting that *SCN8A* mutations are involved in epileptic encephalopathies.[8]

In this study, we performed target capture sequencing or whole-exome sequencing to elucidate the genetic basis of early onset epileptic encephalopathies (EOEEs). We identified de novo *SCN8A* mutations in seven patients with severe epileptic encephalopathies.

Patients and Methods

Patients

A total of 163 patients with EOEEs (48 patients with Ohtahara syndrome, 2 with early myoclonic encephalopathy, 47 with West syndrome, 6 with malignant migrating partial seizures in infancy [MMPSI], and 60 with unclassified EOEEs) were analyzed by target capture sequencing (28 samples) or whole-exome sequencing (135 samples). A total of 98 patients with mutations in *STXBP1*, *ARX*, *KCNQ2*, *SCN1A*, *SCN2A*, *KCNT1*, *CDKL5*, *CASK*, or *MECP2*, which were detected either by high resolution melting analysis, direct sequencing analysis, target capture sequencing, or whole-exome sequencing, were excluded from the study. Therefore, in 163 patients, mutations in the genes described were excluded except for 28 patients examined with target capture sequencing (*KCNT1* was not included in the captured probes used). The diagnosis was made by the clinical features and electroencephalography (EEG) patterns. The experimental protocols were approved by the institutional review board of Yokohama City University School of Medicine and Yamagata University Faculty of Medicine. Peripheral blood samples were obtained from family members after obtaining their written informed consent. Detailed clinical information was obtained from corresponding clinicians.

Target capture sequencing

A custom-made SureSelect oligonucleotide probe library (Agilent Technologies, Santa Clara, CA, U.S.A.) was designed to capture the coding exons of 50 genes, in which additional 15 genes, including *SCN8A*, were added to the panel of the previous 35 genes.[14] A total of 4,764 probes, covering 267 kb, were prepared. Twenty-four captured libraries were mixed and sequenced by the multiplex method on an Illumina MiSeq (Illumina, San Diego, CA, U.S.A.) with 150-bp paired-end reads. Data processing, variant calling, and variant annotation were performed as previously described.[14]

Whole-exome sequencing

Genomic DNA was captured using the SureSelect Human All Exon v4 Kit (51 Mb; Agilent Technologies) and sequenced on an Illumina HiSeq2000 (Illumina) with 101 bp paired-end reads. Four samples were run in one lane of the flow cell. Exome data processing, variant calling, and variant annotation were performed as described previously.[15]

Sanger sequencing

SCN8A mutations identified by target capture sequencing or whole-exome sequencing were confirmed by Sanger sequencing. Parental samples were sequenced to confirm whether parents possessed *SCN8A* mutations.

Results

A total of 7 *SCN8A* mutations were found in 7 patients: 6 of 60 unclassified EOEEs (10.0%), and one of 6 MMPSI cases (16.7%; Table 1). One mutation was identified by target capture sequencing and the other six mutations were found by whole-exome sequencing. They are absent from the 6,500 exomes included in the National Heart, Lung, and Blood Institute exome project and from our 408 in-house control exomes. Sorting Intolerant from Tolerant (SIFT), Polyphen2, and Mutation Taster predicted that the seven mutations were highly damaging to the structure of $Na_v1.6$, and all the seven mutations occurred at evolutionally conserved amino acids (Fig. S1 and Table S1). Two mutations occurred within the same amino acid residue (p.Asn1466): c.4398C>A (p.Asn1466Lys) in patient 1 and c.4397A>C (p.Asn1466Thr) in patient 5 (Fig. 1 and Table 1). The mutations were scattered throughout the entire gene: two in the inactivation gate between domains III and IV, one in a linker between S3 and S4 of domain I, one in S4 of domain II, one in S4 of domain IV, one in a linker between S4 and S5 of domain IV, and one in the C-terminal domain (Fig. 1).

Table 1. Clinical features of patients with *SCN8A* mutations

Clinical Feature	Patient number 1	2	3	4	5	6	7
Age	6 years	13 years	5 years	2 years	6 years	1 year 1 month	1 year 4 months
Sex	Male	Female	Male	Female	Male	Female	Male
Race	Japanese	Japanese	Japanese	Japanese	Israeli	Israeli	Israeli
Diagnosis	EOEE	EOEE	MMPSI	EOEE	EOEE	EOEE	EOEE
Mutation	c.4398C>A (p.Asn1466Lys)	c.647T>A (p.Val216Asp)	c.2537T>C (p.Phe846Ser)	c.4850G>A (p.Arg1617Gln)	c.4397A>C (p.Asn1466Thr)	c.5614C>T (p.Arg1872Trp)	c.4948G>A (p.Ala1650Thr)
Family history	–	–	+	–	+	–	–
Initial symptoms	Seizure	Seizure	Tachypnea and jitteriness (tremor)	Seizure	Seizure	Seizure	Seizure
Age at onset	3 days	7 months	0 days	3 months	4 months	3 months	3.5 months
Epilepsy	Tonic–clonic seizure	Absence seizure	Apneic attacks since 2 months, hemiclonic convulsions propagating to the other side since 4 months	FC at 3 months, tonic –clonic seizure at 6 months	PS with generalization at 4 month, focal tonic and generalized clonic seizures at 1 year, FS with generalization at 5 year	Prolonged tonic–clonic seizure since 3 months	Seizure manifesting as loss of tone and consciousness at 3.5 months, tonic seizure at 5.5 months
Initial EEG	Irregular polyspike-and-slow wave complexes	Focal spikes and 3 Hz generalized spike-and-wave burst	Normal at birth. At 4 months, polyspikes and migrating spike-and-slow wave complex	Normal at 3 months	Normal at 4 months, bilateral temporal sharp waves at 5 months	Multifocal spikes with bilateral discharges	Normal at 5.5 months
Response to therapy	Intractable, PHT+GBP, ACTH, TPM, MDL, LD temporarily effective	Intractable. Seizure-free from 6 years with VPA (now 13 years old)	Intractable, high-dose PB, PHT, LTG, KD, VNS temporarily effective	Intractable CBZ temporarily effective	Intractable, Controlled with TPM and CBZ	Intractable, Controlled with KD+TPM+LCM+ LEV+VGB	Intractable, Controlled with TPM and CBZ
Initial motor development	Delayed	Delayed	Delayed	Delayed	Normal	Delayed	Normal
Development	Severely delayed	Severely delayed	Severely delayed	Severely delayed	Regressed	Severely delayed	Severely regressed
Hypotonia	+ (severe)	+ (5 months)	+	–	–	+	–
Intellectual disability	+ (profound)	+	+ (profound)	+ (profound)	+ (profound)	+ (profound)	+
Behavioral anomalies	+	+	–	–	+	–	–
Current status	Bedridden	Wheelchair	Bedridden	Sitting/crawling	Walking	Unable to sit or crawl, but able to roll over	Bedridden
MRI	MA of CB at 6 months, HI on T2WI in bilateral striatal bodies and occipital cortex	MA of frontal and temporal lobe at 1 year and 10 months	Normal at 0 and 2 months. MA of the CB and thin CC at 9 months and 4 years. MA of the cerebellum at 4 years	Normal at 6 months and 2 years	Normal at 8 months, diffuse brain atrophy at 1 year	Within normal limits, MA	Asymmetric ventricles at 3.5 months, mild diffuse atrophy at 12 months

EOEE, early–onset epileptic encephalopathies; MMPSI, malignant migrating partial seizures in infancy; FC, febrile convulsion; PS, partial seizure; FS, focal seizure; PHT, phenytoin; GBP, gabapentin; ACTH, adrenocorticotrophic hormone; TPM, topiramate; MDL, midazolam; LD, lidocaine; VPA, valproic acid; PB, phenobarbital; LTG, lamotrigine; KD, ketogenic diet; VNS, vagal nerve stimulation; CBZ, carbamazepine; LCM, lacosamide; LEV, levetiracetam; VGB, vigabatrin; HI, hyperintensity; T2WI, T_2-weighted image; MA, mild atrophy; CB, cerebrum; CC, corpus callosum; N.D., not described.

Epilepsia, 55(7):994–1000, 2014
doi: 10.1111/epi.12668

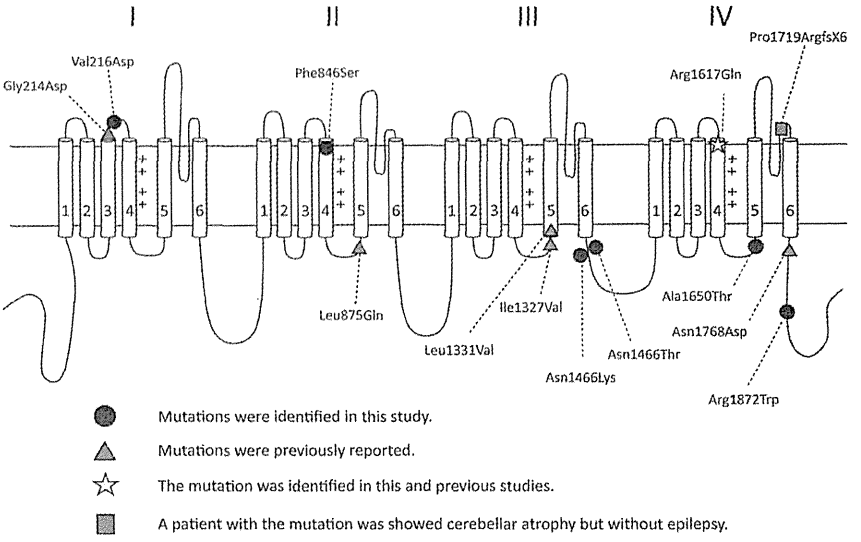

Figure 1.
Structure of the human $Na_v1.6$ channel showing location of *SCN8A* mutations. Mutation annotations are based on NM_014191.3. p.Gly214Asp, p.Leu875Gln, p.Ile1327Val, p.Leu1331Val, p.Arg1617Gln, p.Pro1719ArgfsX6, and p.Asn1768Asp were reported previously.[9–13,25] The patient with p.Pro1719ArgfsX6 showed cerebellar atrophy but without epilepsy.[25]
Epilepsia © ILAE

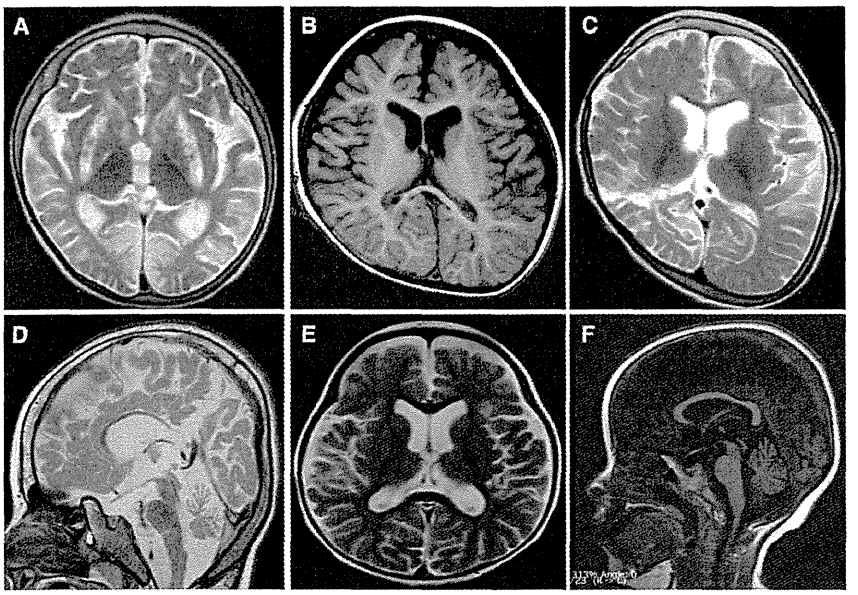

Figure 2.
Brain MRI of patients with *SCN8A* mutations. (**A**, **C**, **E**) T_2-weighted, (**B**) T_1-weighted axial images, (**D**) T_2-weighted, and (**F**) T_1-weighted sagittal images of the patients. (**A**) Patient 1 at 2 years and 11 months; (**B**) patient 2 at 1 year and 10 months; (**C**, **D**) patient 3 at 4 years; (**E**, **F**) patient 4 at 2 years. Hyperintensity in bilateral striatal bodies, and the medial occipital and temporooccipital cortexes was observed in patient 1 (**A**). Patient 2 showed mild atrophy of frontal and temporal lobes (**B**). Patient 3 showed mild brain atrophy with a dilation of the anterior horn of the lateral ventricle and a split of the right hemisphere by parieto-occipitotemporal lobotomy (**C**), as well as a thin corpus callosum and mild cerebellar atrophy (**D**). Patient 4 showed no obvious brain abnormalities (**E**, **F**).
Epilepsia © ILAE

The clinical features of patients with *SCN8A* mutations are summarized in Table 1, and their representative brain images and EEG are shown in Figures 2 and 3. All seven patients showed intractable seizures, developmental delay in infancy, or regression after seizure onset, resulting in severe intellectual disability in later life. In two patients showing developmental regression, some developmental improvements were regained with control of seizures. Four patients showed hypotonia. The onset of seizures and their types were highly variable, and included tonic–clonic seizures at the age of 3 days in patient 1 and 3 months in patient 6, atypical absence seizures at the age of 7 months

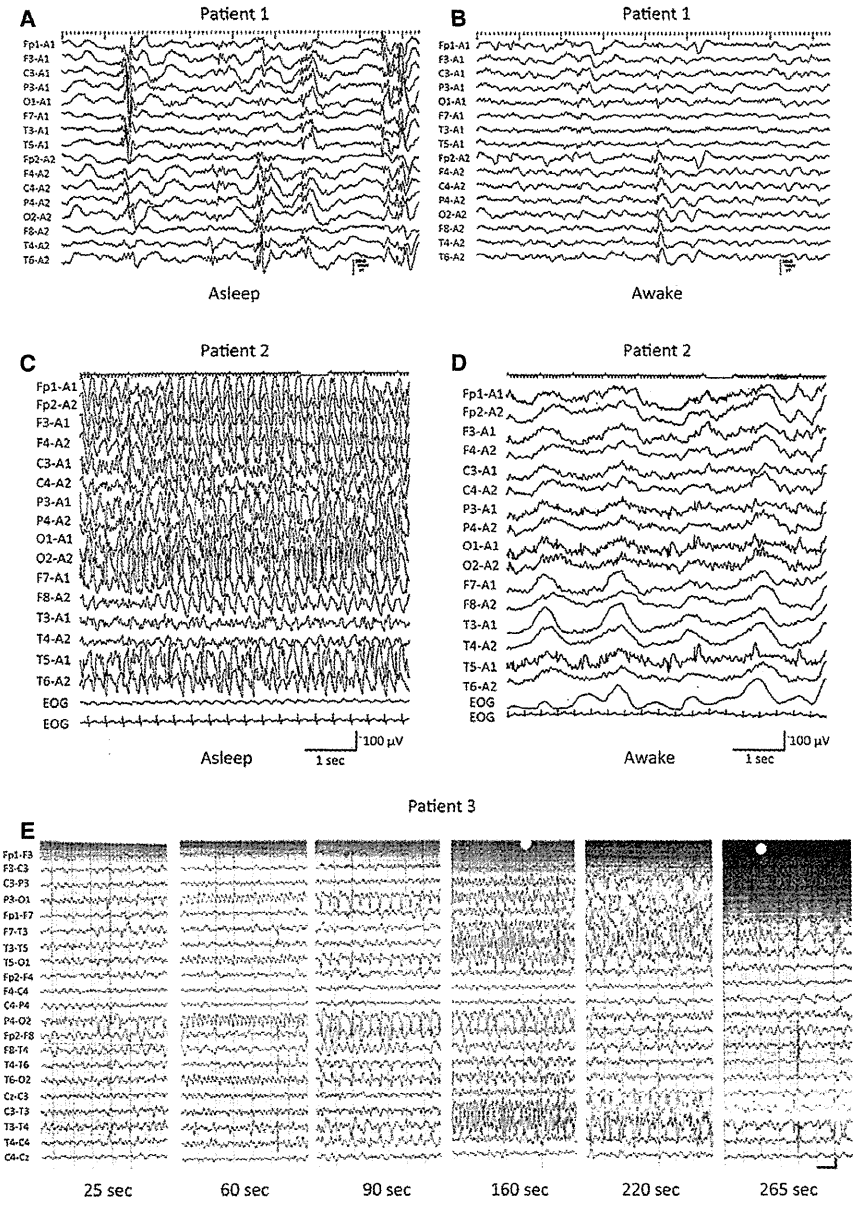

Figure 3.
EEG of patients with *SCN8A* mutations. (**A**, **B**) EEG of patient 1 at the age of 6 months. Diffuse or unilateral hemispheric irregular polyspike-and-slow wave complexes were more frequently seen when asleep (**A**) than awake (**B**). (**C**, **D**) Interictal EEG of patient 2 at the age of 5 years. Electrical status epilepticus was observed when asleep (**C**), and a left occipital predominant areal spike-and-slow wave complex occurred when awake (**D**). (**E**) Ictal EEG of patient 3 at 9 months. Left occipital sharp waves spreading to the right followed by a polyspike or fast wave at T3–T5 were seen in association with an apneic attack and right facial twitching propagating to a right hemiclonic seizure.
Epilepsia © ILAE

(patient 2), apnea attacks at 2 months (patient 3), a febrile convulsion at 3 months (patient 4), partial seizures with secondary generalization at 4 months (patient 5), and seizures manifesting as loss of tone and consciousness at 3.5 months (patient 7). Six patients developed mild cerebral atrophy, and patient 3 showed cerebellar atrophy on brain magnetic resonance imaging (MRI) (Fig. 2). The initial EEG was normal in four patients (patients 3, 4, 5, and 7). A variety of EEG abnormalities was found in patients with *SCN8A* mutations (Fig. 3). Various antiepileptic treatments were only temporarily effective in controlling seizures; however, patient 2 (now 13 years of age) has been seizure free on valproic acid since the age of 6 years, and the seizures of patients 5, 6, and 7 were almost controlled at the last examination with rare breakthrough seizures. In patients 5 and 7, carbamazepine and topiramate combination therapy was effective in controlling seizures. Ketogenic diet was effective in patient 3 who, however, demonstrated severe ileus. Phenytoin, which blocks VGSCs,[16] was used in five patients (patient 1, 2, 3, 5, and 7), showing only temporarily effects at maximum.

Discussion

It has been reported that $Na_v1.2$ (SCN2A) channels are expressed early in development, and that $Na_v1.6$ (SCN8A)

gradually replace $Na_v1.2$ in a population of excitatory neurons during maturation.[16,17] In fact, the developmental shift in splicing of *SCN8A* exon 18 to a transcript encoding the full length protein is still incomplete at 10 months of age.[7] Therefore, it can be postulated that the onset of seizures may be earlier in cases with *SCN2A* mutations compared with *SCN8A* mutations. Our present study supports this hypothesis, as only 2 (28.6%) of 7 cases with *SCN8A* mutations had an onset during the neonatal period, whereas 11 (73.3%) of 15 cases with *SCN2A* mutations previously showed a neonatal seizure onset.[18]

Regarding the functional properties of each domain, at least three types of aberrations appear to be involved: voltage sensing, inactivation, and the interaction of accessory proteins. Two mutations (p.Phe846Ser and p.Arg1617Gln) were located in S4 transmembrane segments, which play a key role in voltage sensing and undergo a conformational change when the pore opens.[1,16] Therefore, these mutations may alter both the activation and inactivation of $Na_v1.6$ consistent with the demonstrated effect on activation of the *SCN8A* mutation Asn1768Asp in domain 4 transmembrane segment 6.[9] Three regions involved in inactivation contained mutations in the present study: the linker between domains III and IV that forms an inactivation gate (p.Asn1466Lys and p.Asn1466Thr),[16,19] the loop between S4 and S5 in domain IV (pAla1650Thr) that forms the inactivation gate receptor together with S6 in domain IV, and the loops between S4 and S5 in domain III (p.Ile1327-Val).[13,19] It is likely that these mutations disturb the inactivation of $Na_v1.6$. One mutation (p.Arg1872Trp) was located in the C-terminal cytoplasmic domain, which is involved in the interaction with accessory proteins such as β-subunits, calmodulin, G protein, and the antiepileptic drug phenytoin.[16,20,21] This mutation is likely to affect the interaction between $Na_v1.6$ and accessory proteins.

Although we attempted to find phenotype–genotype correlations of *SCN8A* mutations based on these functional classifications, no clear correlations could be found. For example, mutations in patients 1 and 5 were located in the same codon (Asn1466) involving channel inactivation, but the onset and type of seizures differed between the two patients (3 days and 4 months). Similarly, patients 3 and 4 both had mutations in the S4 domain, but their clinical courses were quite different. Further study of functional characterization of the effects of de novo mutations on *SCN8A* activity may reveal relationships to clinical course and drug response. Furthermore, a lack of clear phenotype–genotype correlations may suggest the involvement of genetic modifiers. In fact, examples of interactions between channel variants have been described previously; the $Scn8a^{med\text{-}jo/+}$ mutation can rescue the seizures and premature lethality of $Scn1a^{+/-}$ mice, demonstrating the existence of genetic interactions between *Scn1a* and *Scn8a*.[22] In humans, it has been suggested that *SCN9A* is a modifier of *SCN1A*-related epilepsies such as genetic epilepsy with febrile seizure plus and Dravet syndrome.[23,24] Next-generation sequencing has enabled the comprehensive examination of mutations and should provide information about candidate modifier genes.

A nonsense *SCN8A* mutation was reported previously in a patient with intellectual disability, pancerebellar atrophy, and cerebellar ataxia, but without epilepsy.[25] Moreover, mice carrying a homozygous missense mutation in *Scn8a* showed chronic ataxia with an unsteady, wide-based gait,[8,26] supporting the association between *SCN8A* mutations and cerebellar atrophy in humans. In this study, only patient 3 showed cerebellar atrophy. Analysis of a larger group of patients with *SCN8A* mutations is required to validate this issue. One interesting phenotype of *SCN8A* mutations is atypical absence seizures, as seen in patient 2. It was also reported that *Scn8a* heterozygous null mutant mice exhibit spike-wave discharges on their EEG and absence epilepsy.[27] Thus, *SCN8A* might be an important gene for human absence seizures. All the *SCN8A* mutations found in epileptic encephalopathy are missense mutations, which is in striking contrast to the predominance of loss-of-function mutations of *SCN1A* in Dravet syndrome,[28] suggesting that haploinsufficiency is not causal in the case of *SCN8A*, but rather, gain of abnormal function is likely to be involved.

Although five of the patients with an *SCN8A* mutation showed severe developmental delay, two patients showed normal initial development. They showed developmental regression after seizure onset. Of interest, they regained some developmental improvement upon seizure control. This fact indicates that in some patients with a *SCN8A* mutation, control of seizure may ameliorate development.

Dravet syndrome, which is caused by *SCN1A* mutations, shows one of the highest rates of sudden death in patients with epilepsy, ranging from 5.7% to 10% in studied cohorts, and the rate is estimated at about 30-fold higher than in patients with other pediatric-onset epilepsies.[29] Veeramah et al.[9] reported that a patient with a de novo *SCN8A* mutation died from SUDEP at the age of 15 years. Patients in this study are all younger than this and SUDEP is rare in children with epilepsy before the age of 15.[30] However, tonic–clonic seizures, treatment-resistant epilepsy, developmental delay, and neurologic disorders such as intellectual disability and cerebral palsy are all risk factors for SUDEP[30]; most of these risk factors are present in our patients. We suggest that careful follow-up is warranted in patients with *SCN8A* mutations to monitor the potential development of SUDEP.

Acknowledgments

We would like to thank all patients and their families for their participation in this study. We also thank Nobuko Watanabe for her technical assistance. Supported by the Ministry of Health, Labour and Welfare of Japan; the Japan Society for the Promotion of Science (a Grant-in-Aid for Scientific Research [B] from [25293085, 25293235], a Grant-in-Aid for Scientific Research [A] [13313587], a Grant-in-Aid for Scientific Research [C] [24591500]); the Takeda Science Foundation; the Japan Science and

Technology Agency; the Strategic Research Program for Brain Sciences (11105137); and a Grant-in-Aid for Scientific Research on Innovative Areas (Transcription Cycle) from the Ministry of Education, Culture, Sports, Science and Technology of Japan (12024421).

Conflict of Interest

We confirm that we have read the Journal's position on issues involved in ethical publication and affirm that this report is consistent with those guidelines. None of the authors has any conflict of interest to disclose.

References

1. Lai HC, Jan LY. The distribution and targeting of neuronal voltage-gated ion channels. *Nat Rev Neurosci* 2006;7:548–562.
2. Oliva M, Berkovic SF, Petrou S. Sodium channels and the neurobiology of epilepsy. *Epilepsia* 2012;53:1849–1859.
3. Meisler MH, Kearney JA. Sodium channel mutations in epilepsy and other neurological disorders. *J Clin Invest* 2005;115:2010–2017.
4. Whitaker WR, Faull RL, Waldvogel HJ, et al. Comparative distribution of voltage-gated sodium channel proteins in human brain. *Brain Res Mol Brain Res* 2001;88:37–53.
5. Meisler MH, O'Brien JE, Sharkey LM. Sodium channel gene family: epilepsy mutations, gene interactions and modifier effects. *J Physiol* 2010;588:1841–1848.
6. Caldwell JH, Schaller KL, Lasher RS, et al. Sodium channel Na(v)1.6 is localized at nodes of ranvier, dendrites, and synapses. *Proc Natl Acad Sci USA* 2000;97:5616–5620.
7. O'Brien JE, Drews VL, Jones JM, et al. Rbfox proteins regulate alternative splicing of neuronal sodium channel *SCN8A*. *Mol Cell Neurosci* 2012;49:120–126.
8. O'Brien JE, Meisler MH. Sodium channel *SCN8A* (Nav1.6): properties and *de novo* mutations in epileptic encephalopathy and intellectual disability. *Front Genet* 2013;4:213.
9. Veeramah KR, O'Brien JE, Meisler MH, et al. De novo pathogenic *SCN8A* mutation identified by whole-genome sequencing of a family quartet affected by infantile epileptic encephalopathy and SUDEP. *Am J Hum Genet* 2012;90:502–510.
10. Allen AS, Berkovic SF, Cossette P, et al. *De novo* mutations in epileptic encephalopathies. *Nature* 2013;501:217–221.
11. Carvill GL, Heavin SB, Yendle SC, et al. Targeted resequencing in epileptic encephalopathies identifies *de novo* mutations in *CHD2* and *SYNGAP1*. *Nat Genet* 2013;45:825–830.
12. Rauch A, Wieczorek D, Graf E, et al. Range of genetic mutations associated with severe non-syndromic sporadic intellectual disability: an exome sequencing study. *Lancet* 2012;380:1674–1682.
13. Vaher U, Noukas M, Nikopensius T, et al. *De novo SCN8A* mutation identified by whole-exome sequencing in a boy with neonatal epileptic encephalopathy, multiple congenital anomalies, and movement disorders. *J Child Neurol* 2013; Dec 18 [Epub ahead of print].
14. Kodera H, Kato M, Nord AS, et al. Targeted capture and sequencing for detection of mutations causing early onset epileptic encephalopathy. *Epilepsia* 2013;54:1262–1269.
15. Saitsu H, Nishimura T, Muramatsu K, et al. *De novo* mutations in the autophagy gene *WDR45* cause static encephalopathy of childhood with neurodegeneration in adulthood. *Nat Genet* 2013;45:445–449, 9e1.
16. Eijkelkamp N, Linley JE, Baker MD, et al. Neurological perspectives on voltage-gated sodium channels. *Brain* 2012;135:2585–2612.
17. Liao Y, Deprez L, Maljevic S, et al. Molecular correlates of age-dependent seizures in an inherited neonatal-infantile epilepsy. *Brain* 2010;133:1403–1414.
18. Nakamura K, Kato M, Osaka H, et al. Clinical spectrum of *SCN2A* mutations expanding to Ohtahara syndrome. *Neurology* 2013;81:992–998.
19. Catterall WA. From ionic currents to molecular mechanisms: the structure and function of voltage-gated sodium channels. *Neuron* 2000;26:13–25.
20. Rusconi R, Scalmani P, Cassulini RR, et al. Modulatory proteins can rescue a trafficking defective epileptogenic Nav1.1 Na+ channel mutant. *J Neurosci* 2007;27:11037–11046.
21. Vacher H, Trimmer JS. Trafficking mechanisms underlying neuronal voltage-gated ion channel localization at the axon initial segment. *Epilepsia* 2012;53(Suppl. 9):21–31.
22. Martin MS, Tang B, Papale LA, et al. The voltage-gated sodium channel *Scn8a* is a genetic modifier of severe myoclonic epilepsy of infancy. *Hum Mol Genet* 2007;16:2892–2899.
23. Singh NA, Pappas C, Dahle EJ, et al. A role of *SCN9A* in human epilepsies, as a cause of febrile seizures and as a potential modifier of Dravet syndrome. *PLoS Genet* 2009;5:e1000649.
24. Mulley JC, Hodgson B, McMahon JM, et al. Role of the sodium channel *SCN9A* in genetic epilepsy with febrile seizures plus and Dravet syndrome. *Epilepsia* 2013;54:e122–e126.
25. Trudeau MM, Dalton JC, Day JW, et al. Heterozygosity for a protein truncation mutation of sodium channel *SCN8A* in a patient with cerebellar atrophy, ataxia, and mental retardation. *J Med Genet* 2006;43:527–530.
26. Meisler MH, Plummer NW, Burgess DL, et al. Allelic mutations of the sodium channel SCN8A reveal multiple cellular and physiological functions. *Genetica* 2004;122:37–45.
27. Papale LA, Beyer B, Jones JM, et al. Heterozygous mutations of the voltage-gated sodium channel *SCN8A* are associated with spike-wave discharges and absence epilepsy in mice. *Hum Mol Genet* 2009;18:1633–1641.
28. Escayg A, Goldin AL. Sodium channel *SCN1A* and epilepsy: mutations and mechanisms. *Epilepsia* 2010;51:1650–1658.
29. Kalume F. Sudden unexpected death in Dravet syndrome: respiratory and other physiological dysfunctions. *Respir Physiol Neurobiol* 2013;189:324–328.
30. Devinsky O. Sudden, unexpected death in epilepsy. *N Engl J Med* 2011;365:1801–1811.

Supporting Information

Additional Supporting Information may be found in the online version of this article:

Appendix S1. Case reports.

Table S1. Prediction of Mutation Pathogenicity.

Figure S1. Conservation of substituted amino acids by *SCN8A* mutations.

Available online at www.sciencedirect.com

ScienceDirect

Neuromuscular Disorders 24 (2014) 642–647

www.elsevier.com/locate/nmd

Case report

Deep sequencing detects very-low-grade somatic mosaicism in the unaffected mother of siblings with nemaline myopathy

Satoko Miyatake [a,1], Eriko Koshimizu [a,1], Yukiko K. Hayashi [b,c], Kazushi Miya [d], Masaaki Shiina [e], Mitsuko Nakashima [a], Yoshinori Tsurusaki [a], Noriko Miyake [a], Hirotomo Saitsu [a], Kazuhiro Ogata [e], Ichizo Nishino [b], Naomichi Matsumoto [a,*]

[a] *Department of Human Genetics, Yokohama City University Graduate School of Medicine, Yokohama, Japan*
[b] *Department of Neuromuscular Research, National Institute of Neuroscience, National Center of Neurology and Psychiatry, Tokyo, Japan*
[c] *Department of Neurophysiology, Tokyo Medical University, Tokyo, Japan*
[d] *Department of Pediatrics, Faculty of Medicine, University of Toyama, Toyama, Japan*
[e] *Department of Biochemistry, Yokohama City University Graduate School of Medicine, Yokohama, Japan*

Received 12 December 2013; received in revised form 1 April 2014; accepted 11 April 2014

Abstract

When an expected mutation in a particular disease-causing gene is not identified in a suspected carrier, it is usually assumed to be due to germline mosaicism. We report here very-low-grade somatic mosaicism in *ACTA1* in an unaffected mother of two siblings affected with a neonatal form of nemaline myopathy. The mosaicism was detected by deep resequencing using a next-generation sequencer. We identified a novel heterozygous mutation in *ACTA1*, c.448A>G (p.Thr150Ala), in the affected siblings. Three-dimensional structural modeling suggested that this mutation may affect polymerization and/or actin's interactions with other proteins. In this family, we expected autosomal dominant inheritance with either parent demonstrating germline or somatic mosaicism. Sanger sequencing identified no mutation. However, further deep resequencing of this mutation on a next-generation sequencer identified very-low-grade somatic mosaicism in the mother: 0.4%, 1.1%, and 8.3% in the saliva, blood leukocytes, and nails, respectively. Our study demonstrates the possibility of very-low-grade somatic mosaicism in suspected carriers, rather than germline mosaicism.

Keywords: Nemaline myopathy; *ACTA1*; Deep resequencing; Next-generation sequencer; Low-grade somatic mosaicism

1. Introduction

Nemaline myopathy is a common form of congenital myopathy characterized clinically by general hypotonia and muscle weakness, and pathologically by the presence of nemaline bodies within the myofibers [1,2]. *ACTA1* is one of the nine known genes associated with nemaline myopathy [3].

Sometimes in the clinic, an expected mutation is not identified in a suspected carrier. This is usually assumed to be because of germline mosaicism, in which mosaicism occurs in the carrier's germline only. Here we report, for the first time, very-low-grade somatic mosaicism detected by deep resequencing using a next-generation sequencer (NGS) in an unaffected mother of two affected siblings.

* Corresponding author. Address: Department of Human Genetics, Yokohama City University Graduate School of Medicine, 3-9 Fukuura, Kanazawa-ku, Yokohama 236-0004, Japan, Tel.: +81 45 787 2604; fax: +81 45 786 5219.
E-mail address: naomat@yokohama-cu.ac.jp (N. Matsumoto).
[1] These authors contributed equally.

http://dx.doi.org/10.1016/j.nmd.2014.04.002
0960-8966/

2. Case report

2.1. The proband

The proband was a boy who was 6 years old at the time of the study. He was the first child of healthy nonconsanguineous Japanese parents. He had an affected sister (Fig. 1a). He was born by cesarean section at 40 weeks of gestation after an uneventful pregnancy. He was admitted to a neonatal intensive care unit immediately after birth because of asphyxia with loss of spontaneous respiration and general hypotonia. His birth weight was 2640 g, height 48 cm, and occipitofrontal head circumference 33 cm. His Apgar scores were 1 and 4 at 1 and 5 min, respectively. He quickly recovered with ventilatory support. Laboratory tests showed normal findings except mildly elevated creatine kinase (653 IU/L). When he was discharged at age 2 months, general hypotonia remained with absent deep tendon reflexes. Antigravity movements were not observed. Arthrogryposis and mild cardiomegaly were noted. Ultrasound cardiography revealed mild dilatation and dyskinesia of the left ventricle. At 7 months, he was given a tracheostomy, and home ventilation therapy was introduced because of aspiration pneumonia (Supplementary Fig. 1a). Tube-feeding was also started because of poor swallowing. At 9 months, a muscle biopsy was performed. On a modified Gomori trichrome stain, nearly all the muscle fibers contained nemaline rods. Intranuclear rods were also scattered (Fig. 1b). On staining for ATPases, type 1 fiber atrophy and predominance were seen. Immunolabeling of a muscle biopsy from the patient with α-actinin showed intensely stained rod bodies (Fig. 1c). Co-staining with α-actinin, lamin A (as a marker of the nuclear envelope), and DAPI clearly revealed intranuclear rods (Fig. 1c). His condition was diagnosed as nemaline myopathy. He could sit unassisted at age 2 years, move on his hip at age 3, and walk with assistance at age 5. He showed normal intellectual ability. At 5 years, his cardiac function was re-evaluated by ultrasound cardiography. Mild left ventricular dilatation and dyskinesia remained.

2.2. The affected sister

The proband's only sibling, a sister 3 years younger, was also affected (Fig. 1a). She was born by cesarean section at 38 weeks of gestation after an uneventful pregnancy. She was similarly admitted to a neonatal intensive care unit immediately after birth because of hypoventilation and hypotonia. Her birth weight was 2620 g, height 48.5 cm, and occipitofrontal head circumference 36.5 cm. Her Apgar scores were 4 and 6 at 1 and 5 min, respectively. Serum creatine kinase was 190 IU/L, which was within the normal range. She recovered with ventilatory support, but needed continuous oxygen therapy. She had difficulty thriving and tube-feeding was introduced. Her cardiac function was normal without cardiomegaly. General hypotonia remained. After she was discharged at age 2 months, frequent aspiration pneumonia occurred. She started to use nocturnal noninvasive positive pressure ventilation at the age of 22 months. At age 2 years, she was given a tracheostomy and was controlled under nocturnal ventilation after respiratory syncytial virus infection following respiratory failure (Supplementary Fig. 1a). Because of her clinical presentation, she was also suggested to have congenital (nemaline) myopathy. At present, she shows antigravity movement of the extremities although she has not acquired head control and cannot roll over.

2.3. Genetic and three-dimensional structural analysis

First we checked for *ACTA1* (NM_001100.3) mutation in the proband's DNA, considering the presence of intranuclear rods. We identified a novel heterozygous missense mutation, c.448A>G (p.Thr150Ala), by Sanger sequencing. Because autosomal recessive inheritance was possible from the family tree, we performed whole-exome sequencing of the proband, affected sister, and their parents to identify a further genetic cause. Genomic DNA obtained from blood leukocytes was captured using a SureSelect^{XT} Human All Exon 50 Mb Kit (Agilent Technologies, Santa Clara, CA) and sequenced on a HiSeq2000 (Illumina, San Diego, CA) with 101-bp paired-end reads, as previously described [4]. The mean depth of coverage was 123× to 143×. We selected rare protein-altering and splice-site variants after filtering against dbSNP135 and 408 in-house control exomes. Among the rare variant calls, we first screened for genes known to cause nemaline myopathies, namely *ACTA1* (MIM 102610) [3], *TPM3* (MIM 191030) [5], *NEB* (MIM 161650) [6], *TPM2* (MIM 190990) [7], *TNNT1* (MIM 191041) [8], *CFL2* (MIM 601443) [9], *KBTBD13* (MIM 613727) [10], *KLHL40* (MIM 615340) [11], and *KLHL41* (MIM 607701) [12]. We identified only the novel heterozygous missense mutation c.448A>G (p.Thr150Ala) in *ACTA1* in both the affected brother and sister, which we confirmed by Sanger sequencing. Copy number analysis by eXome Hidden Markov Model (XHMM) [13] using next-generation sequencing (NGS) data revealed that there were no copy number changes within the *ACTA1* locus (Supplementary Fig. 1b). This mutation was not identified in either of the parents, after testing DNA obtained from their saliva, hair, nails, and blood by Sanger sequencing (Fig. 2a). This mutation, which alters the evolutionarily well-conserved Thr150 to Ala (Fig. 2b), was not present in the NHLBI Exome Sequencing Project (ESP6500). Two of three web-based prediction programs suggested that this mutation is pathogenic (PolyPhen-2: benign; SIFT: deleterious; MutationTaster: disease-causing). We also searched for any rare variants that were compatible with an autosomal recessive inheritance model, such as a homozygous mutation or compound heterozygous

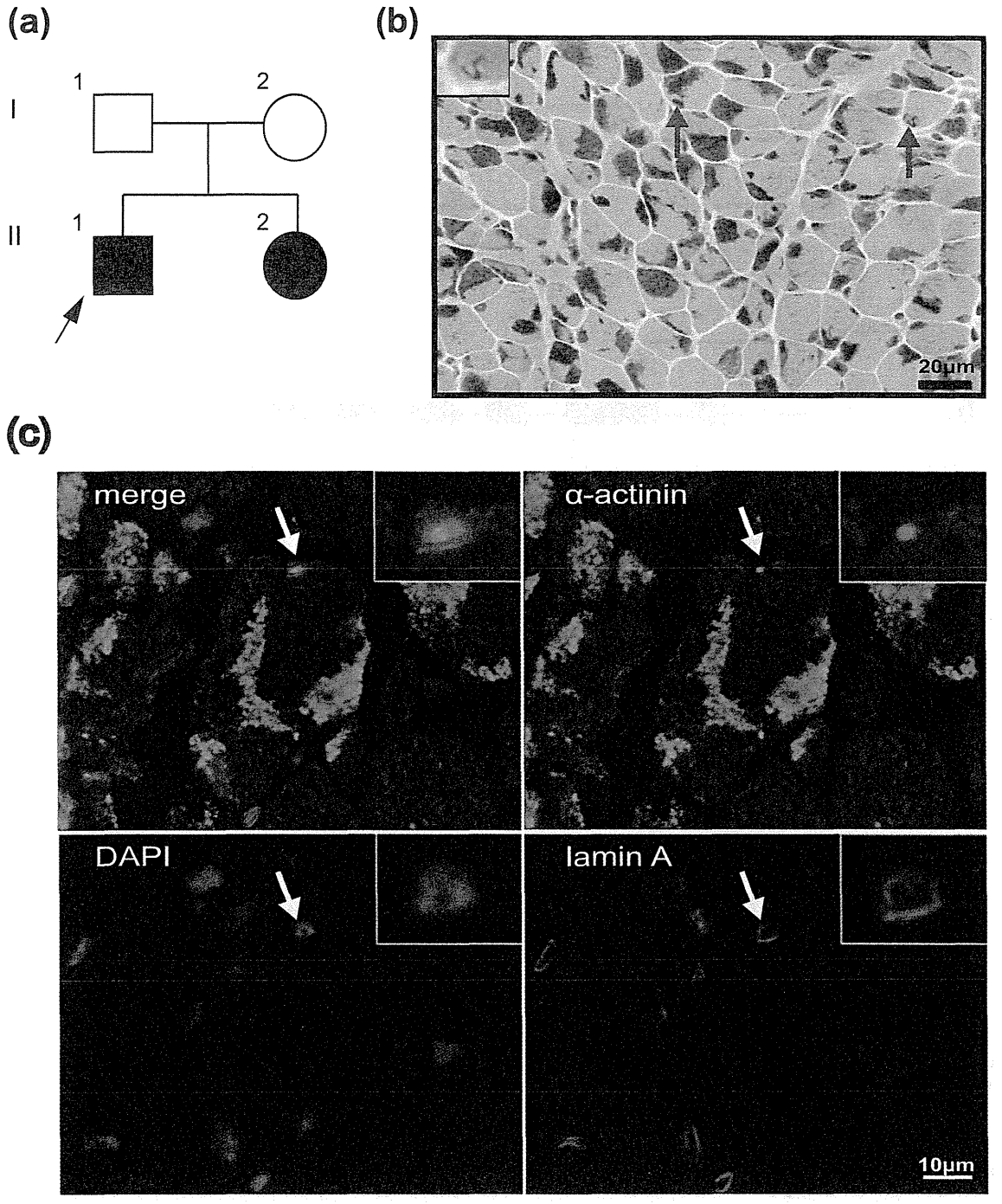

Fig. 1. (a) Family pedigree. (b) Light microscopic images of the muscle of the proband at age 9 months. With a modified Gomori trichrome stain, nearly all the muscle fibers can be seen to contain nemaline rods. Intranuclear rods (arrows, and upper-left window) are also scattered in some nuclei. Bar = 20 μm. (c) Immunohistochemical analysis of a muscle biopsy using anti-α-actinin (EA-53; Sigma, St. Louis, MO) (green) and anti-lamin A (red) antibodies [19]. Nuclei were stained with DAPI (blue). Nemaline rods were strongly stained by anti-α-actinin. An intranuclear rod was also seen (arrows, and higher-magnification inset boxes). Scale bar = 10 μm.

mutation, but no candidate mutations were identified (data not shown).

To explore the effect of the *ACTA1* p.Thr150Ala mutation, we mapped the mutation onto reported crystal structures. Thr150 is located near the polymerization/interaction interfaces between actin monomers (Fig. 2c) and between actin and its interacting proteins (Fig. 2d, Supplementary Fig. 1c). Thus, p.Thr150Ala may

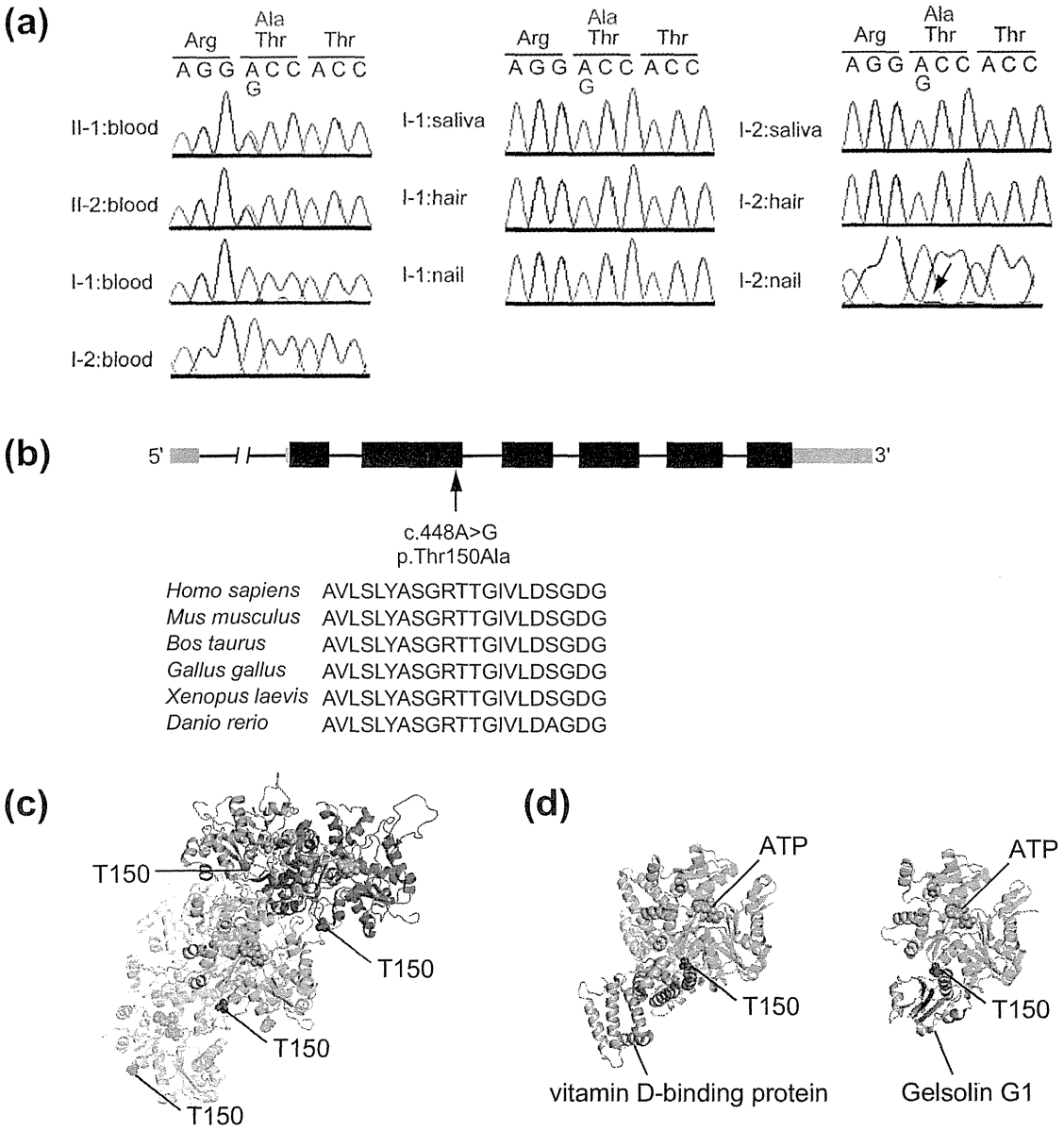

Fig. 2. (a) Sanger sequencing of the c.448A>G mutation using DNA from the affected siblings and the parents obtained from blood (left), and DNA from the father (middle) and mother (right) obtained from saliva, hair, and nails. The heterozygous mutation was identified in the affected siblings but not in any of the parental samples. No clear peak for the G allele was observed in the mother's nail DNA sample (arrow). (b) Schematic representation of *ACTA1*. The light gray bars represent untranslated regions and the black bars represent coding exons. Exon 1 is a non-coding exon. The c.448A>G mutation changes the well-conserved amino acid Thr150 (red) into Ala. (c, d) Structural implications of the p.Thr150Ala mutation in *ACTA1*. Structures of bare F-actin filaments determined by electron microscopy (Protein Data Bank (PDB) code 4A7N) (c) and G-actins in complex with vitamin D-binding protein (PDB code 1KXP) or gelsolin G1 (PDB code 1EQY) (d) are shown. The actin molecules are color-coded to discriminate each monomer in the F-actin filaments or are colored green in the G-actin complexes. Thr150 and ATP molecules are shown as red and pink space-filling spheres, respectively.

affect polymerization and/or the interactions of actin with other proteins.

We expected autosomal dominant inheritance from either parent. To test this, we performed deep resequencing for this mutation using an Illumina MiSeq platform. We used DNAs from the blood of the affected siblings, and from the saliva, nails, hair, and blood of their parents. The total read depth at c.448A in *ACTA1* was 131495× to 425933×. Very-low-grade somatic mosaicism was confirmed in the mother: 0.4%, 1.1%, and 8.3% in saliva, blood, and nails, respectively (all beyond 0.1% of the background level) (Table 1).

We used allele-specific PCR to confirm the presence of the mutation in the mother. The primer sequences and

Table 1
Deep resequencing of c.448A>G in *ACTA1* in various samples from each individual.

Individual	Tissue	Total depth (×)	Disease status	Wild-type allele (×)	Mutant allele (×)	% of wild-type allele	% of mutant allele
II-1 (Proband)	Blood	380016	Affected	192510	186808	50.7	49.2
II-2 (Sister)	Blood	425933	Affected	215496	209612	50.6	49.2
I-1 (Father)	Blood	261948	Unaffected	260897	355	99.6	0.1
I-2 (Mother)	Blood	364850	Unaffected	360030	4103	98.7	1.1
I-1 (Father)	Saliva	245895	Unaffected	245130	299	99.7	0.1
I-1 (Father)	Hair	190636	Unaffected	189929	253	99.6	0.1
I-1 (Father)	Nail	325282	Unaffected	324198	381	99.7	0.1
I-2 (Mother)	Saliva	239339	Unaffected	237872	999	99.4	0.4
I-2 (Mother)	Hair	324289	Unaffected	323120	400	99.6	0.1
I-2 (Mother)	Nail	131495	Unaffected	120210	10956	91.4	8.3

PCR conditions are available upon request. Both the wild-type and mutant alleles were amplified in the proband and the affected sister at a similar level. Both alleles could also be amplified in the mother, but the wild-type allele was amplified at a much greater level than the mutant allele. The wild-type allele only was amplified in the father (Supplementary Fig. 2a). Sanger sequencing of these amplicons confirmed the mutation in the proband, sister, and mother (Supplementary Fig. 2b).

There are various conventional methods to detect somatic mosaicism: Sanger sequencing to detect a small variant peak compared with the wild-type peak, high-resolution melting (HRM) analysis to detect an aberrant melting pattern, allele-specific PCR to amplify only the mutant allele, and pyrosequencing and SNaPshot analysis for quantitative variant detection [14]. We explored whether our very-low-grade somatic mosaicism could be detected by HRM, because this has been suggested to be one of the more sensitive methods [15]. We performed HRM analysis as previously described [16] using DNAs from normal controls, the affected siblings, the father (all DNA derived from blood), and the mother (DNA derived from the nails, which showed the highest rate of mosaicism (8.3%). The melting curves of both affected siblings were aberrant and were called mutant, but those of the father and mother were called normal (Supplementary Fig. 2c). In other words, this technique could not detect the 8.3% mosaicism.

3. Discussion

Here, we report very-low-grade somatic mosaicism in the unaffected mother of siblings with nemaline myopathy, identified by deep resequencing using NGS. Our study is significant in two ways. First, we demonstrate the possibility of very-low-grade somatic mosaicism in a suspected carrier, rather than germline mosaicism; this is likely to be a very rare event. Second, we present another example of the clinical application of NGS.

The novel heterozygous mutation c.448A>G (p.Thr150Ala) in *ACTA1* is likely to be responsible for the nemaline myopathy in this pedigree based on four lines of evidence: the mutation is not registered in the ESP6500 database, the substituted amino acid is well conserved, two previously reported mutations also involve residue 150 (Thr150Asn, Thr150Ser) [17,18], and three-dimensional structural modeling suggests an impact on polymerization and/or the interactions of actin with other proteins. Interestingly, the mutation exists within a region where most of the mutations identified in patients with intranuclear rod myopathy, a variant of nemaline myopathy associated with *ACTA1*, are located [18].

The majority of reported *ACTA1* mutations are *de novo* heterozygous mutations in sporadic cases. This is likely to be due to the severity of nemaline myopathy with *ACTA1* mutation. However, autosomal dominant inheritance has been observed in a few situations: a pedigree with a relatively mild phenotype or incomplete penetrance, or parental somatic/germline mosaicism [2,18]. To date, there have been three reported cases of somatic mosaicism of *ACTA1* in one parent of a severely affected patient [18].

In our study, allele-specific PCR, despite being non-quantitative, was sufficiently sensitive to detect mosaicism in blood leukocytes from the mother (mosaic rate 1.1%). Thus, this method is worth trying to confirm a suspected low-grade mosaicism. In contrast, as we were unable to detect 8.3% mosaicism using HRM, NGS should be the first choice for detecting very-low-grade somatic mosaicism that other methods might miss. A recent paper has described using NGS to detect somatic *BRAF* mutations down to 2% allele frequency, demonstrating the increased sensitivity of this method compared with HRM (limit 6.6% allele frequency), pyrosequencing (limit 5% allele frequency), and Sanger sequencing (limit 6.6% allele frequency) [15].

In our family, the mother does not seem to have any neurological problems in her daily activities, although she has not been clinically examined and no muscle imaging studies or biopsies have been undertaken.

The proband had mild left ventricular dilatation with dyskinesia without a hypertrophic phenotype. In the literature, cardiomegaly appears to be a rare complication. Patients with *ACTA1* mutation usually have hypertrophic cardiomegaly [18,19].

In conclusion, we used NGS to confirm very-low-grade somatic mosaicism in the mother. Using conventional methods, the mother might have been judged to have germline mosaicism. Clinically, our data on the rate of

somatic mosaicism could be used to estimate the recurrence risk, although prenatal diagnosis would be required to provide certainty.

Acknowledgments

We thank all the participants for their cooperation in this research. We also thank Ms. K. Takabe and Mr. T. Miyama, from the Department of Human Genetics, Yokohama City University Graduate School of Medicine, for their technical assistance. This work was supported by grants from the Ministry of Health, Labour and Welfare of Japan (N. Miyake, N. Matsumoto), a Grant-in-Aid for Scientific Research (A) from the Japan Society for the Promotion of Science (N. Matsumoto), a Grant-in-Aid for Scientific Research (B) from the Japan Society for the Promotion of Science (N. Miyake, H.S.), a Grant-in-Aid for Young Scientists (B) (E.K.), a research grant from the Yokohama Foundation for Advancement of Medical Science (S.M.), the Takeda Science Foundation (N. Miyake, H.S., N. Matsumoto), the Fund for the Creation of Innovation Centers for Advanced Interdisciplinary Research Areas Program in the Project for Developing Innovation Systems (N. Matsumoto), the Strategic Research Program for Brain Sciences (E.K., N. Matsumoto), a Grant-in-Aid for Scientific Research on Innovative Areas (Transcription Cycle) from the Ministry of Education, Culture, Sports, Science, and Technology of Japan (N. Miyake, N. Matsumoto), a Grant-in-Aid for Research on Intractable Diseases, Comprehensive Research on Disability, Health and Welfare (Y.K.H., I.N.), a Grant-in-Aid for Applying Health Technology (Y.K.H., I.N.) from the Ministry of Health, Labour and Welfare, Japan, and an Intramural Research Grant 23-5 for Neurological and Psychiatric Disorders of NCNP (I.N.).

Appendix A. Supplementary data

Supplementary data associated with this article can be found, in the online version, at http://dx.doi.org/10.1016/j.nmd.2014.04.002.

References

[1] Nance JR, Dowling JJ, Gibbs EM, Bonnemann CG. Congenital myopathies: an update. Curr Neurol Neurosci Rep 2012;12:165–74.
[2] Romero NB, Sandaradura SA, Clarke NF. Recent advances in nemaline myopathy. Curr Opin Neurol 2013;26:519–26.
[3] Nowak KJ, Wattanasirichaigoon D, Goebel HH, et al. Mutations in the skeletal muscle alpha-actin gene in patients with actin myopathy and nemaline myopathy. Nat Genet 1999;23:208–12.
[4] Nakamura K, Kodera H, Akita T, et al. De novo mutations in GNAO1, encoding a galphao subunit of heterotrimeric g proteins, cause epileptic encephalopathy. Am J Hum Genet 2013;93:496–505.
[5] Laing NG, Wilton SD, Akkari PA, et al. A mutation in the alpha tropomyosin gene TPM3 associated with autosomal dominant nemaline myopathy. Nat Genet 1995;9:75–9.
[6] Pelin K, Hilpela P, Donner K, et al. Mutations in the nebulin gene associated with autosomal recessive nemaline myopathy. Proc Natl Acad Sci USA 1999;96:2305–10.
[7] Donner K, Ollikainen M, Ridanpaa M, et al. Mutations in the beta-tropomyosin (TPM2) gene – a rare cause of nemaline myopathy. Neuromuscul Disord 2002;12:151–8.
[8] Johnston JJ, Kelley RI, Crawford TO, et al. A novel nemaline myopathy in the Amish caused by a mutation in troponin T1. Am J Hum Genet 2000;67:814–21.
[9] Agrawal PB, Greenleaf RS, Tomczak KK, et al. Nemaline myopathy with minicores caused by mutation of the CFL2 gene encoding the skeletal muscle actin-binding protein, cofilin-2. Am J Hum Genet 2007;80:162–7.
[10] Sambuughin N, Yau KS, Olive M, et al. Dominant mutations in KBTBD13, a member of the BTB/Kelch family, cause nemaline myopathy with cores. Am J Hum Genet 2010;87:842–7.
[11] Ravenscroft G, Miyatake S, Lehtokari VL, et al. Mutations in KLHL40 are a frequent cause of severe autosomal-recessive nemaline myopathy. Am J Hum Genet 2013;93:6–18.
[12] Gupta VA, Ravenscroft G, Shaheen R, et al. Identification of KLHL41 mutations implicates BTB-Kelch-mediated ubiquitination as an alternate pathway to myofibrillar disruption in nemaline myopathy. Am J Hum Genet 2013;93:1108–17.
[13] Fromer M, Moran JL, Chambert K, et al. Discovery and statistical genotyping of copy-number variation from whole-exome sequencing depth. Am J Hum Genet 2012;91:597–607.
[14] Tasca G, Fattori F, Ricci E, et al. Somatic mosaicism in TPM2-related myopathy with nemaline rods and cap structures. Acta Neuropathol 2013;125:169–71.
[15] Ihle MA, Fassunke J, Konig K, et al. Comparison of high resolution melting analysis, pyrosequencing, next generation sequencing and immunohistochemistry to conventional Sanger sequencing for the detection of p. V600E and non-p.V600E BRAF mutations. BMC Cancer 2014;14:13.
[16] Miyatake S, Miyake N, Touho H, et al. Homozygous c.14576G>A variant of RNF213 predicts early-onset and severe form of moyamoya disease. Neurology 2012;78:803–10.
[17] Sparrow JC, Nowak KJ, Durling HJ, et al. Muscle disease caused by mutations in the skeletal muscle alpha-actin gene (ACTA1). Neuromuscul Disord: NMD 2003;13:519–31.
[18] Laing NG, Dye DE, Wallgren-Pettersson C, et al. Mutations and polymorphisms of the skeletal muscle alpha-actin gene (ACTA1). Hum Mutat 2009;30:1267–77.
[19] Nowak KJ, Ravenscroft G, Laing NG. Skeletal muscle alpha-actin diseases (actinopathies): pathology and mechanisms. Acta Neuropathol 2013;125:19–32.

Neurogenetics (2014) 15:193–200
DOI 10.1007/s10048-014-0408-y

ORIGINAL ARTICLE

Novel compound heterozygous *PIGT* mutations caused multiple congenital anomalies-hypotonia-seizures syndrome 3

Mitsuko Nakashima · Hirofumi Kashii · Yoshiko Murakami · Mitsuhiro Kato · Yoshinori Tsurusaki · Noriko Miyake · Masaya Kubota · Taroh Kinoshita · Hirotomo Saitsu · Naomichi Matsumoto

Received: 21 February 2014 / Accepted: 25 May 2014 / Published online: 8 June 2014

Abstract Recessive mutations in genes of the glycosylphosphatidylinositol (GPI)-anchor synthesis pathway have been demonstrated as causative of GPI deficiency disorders associated with intellectual disability, seizures, and diverse congenital anomalies. We performed whole exome sequencing in a patient with progressive encephalopathies and multiple dysmorphism with hypophosphatasia and identified novel compound heterozygous mutations, c.250G>T (p. Glu84*) and c.1342C>T (p. Arg488Trp), in *PIGT* encoding a subunit of the GPI transamidase complex. The surface expression of GPI-anchored proteins (GPI-APs) on patient granulocytes was lower than that of healthy controls. Transfection of the Arg488Trp mutant *PIGT* construct, but not the Glu84* mutant, into PIGT-deficient cells partially restored the expression of GPI-APs DAF and CD59. These results indicate that *PIGT* mutations caused neurological impairment and multiple congenital anomalies in this patient.

M. Nakashima · Y. Tsurusaki · N. Miyake · H. Saitsu · N. Matsumoto (✉)
Department of Human Genetics, Yokohama City University Graduate School of Medicine, 3-9 Fukuura, Kanazawa-ku, Yokohama 236-0004, Japan
e-mail: naomat@yokohama-cu.ac.jp

H. Kashii · M. Kubota
Division of Neurology, National Center for Child Health and Development, Tokyo, Japan

Y. Murakami · T. Kinoshita
Research Institute for Microbial Diseases and World Premier International Immunology Frontier Research Center, Osaka University, Osaka, Japan

M. Kato
Department of Pediatrics, Yamagata University Faculty of Medicine, Yamagata, Japan

Keywords Whole exome sequencing · *PIGT* · Compound heterozygous mutations · Glycosylphosphatidylinositol-anchored protein · Multiple congenital anomalies-hypotonia-seizures syndrome 3 · Hypophosphatasia

Introduction

Glycosylphosphatidylinositol (GPI) acts as the anchor of various eukaryotic proteins expressed on the plasma membrane. GPI synthesis and GPI-anchored protein (GPI-AP) modification are mediated by at least 27 genes in the endoplasmic reticulum (ER) and Golgi apparatus [1]. Recent studies have indicated that inherited loss-of-function mutations in these genes lead to GPI deficiencies associated with neurological impairments including seizures, intellectual disability, and multiple congenital anomalies [2–9]. In addition, somatic mutations in PIGA cause paroxysmal nocturnal haemoglobinuria, a haematopoietic disease, which is also caused by somatic mutation of PIGT in combination with the germ line mutation of one allele [10, 11].

PIGT is one of the subunits of the GPI transamidase complex, and catalyzes the attachment of GPI anchors to proteins in the ER [1]. Kvarnung et al. [12] previously reported a homozygous *PIGT* mutation in patients from a consanguineous Turkish family with multiple congenital anomalies-hypotonia-seizures syndrome-3 (MCAHS3 [MIM 615398]). In the present study, we describe the use of whole exome sequencing to identify novel compound heterozygous *PIGT* mutations in a Japanese patient with seizures, intellectual disability and multiple congenital anomalies. Functional analysis indicated that these mutations are causative of GPI deficiency.

Patient and methods

Patient

The female proband was born at full term without asphyxia as the first child of healthy unrelated parents (Fig. 1a). Polyhydramnios was recognized during pregnancy. She showed poor sucking and post-feed stridor soon after birth. At 4 months of age, she showed tonic seizures with apnea and myoclonic seizures, both of which repeatedly turned to convulsive status. Her electroencephalogram (EEG) demonstrated high-amplitude slow wave as a background activity, but no epileptic discharges were observed. She also showed a poor response, muscle hypotonia, unstable head control, a cardiac murmur caused by patent ductus arteriosus, and left hydronephroureter with ureteral stenosis. Her seizures were refractory to multiple antiepileptic drugs such as carbamazepine, clobazam, and an intravenous injection of pyridoxal phosphate while the frequency of her seizures decreased with the combination of valproic acid, zonisamide, and phenytoin to some extent. Phenobarbital could not be used in infancy because of drug eruption. After 1 year of age, she was frequently admitted to hospital because of convulsive status epilepticus induced by fever, or recurrent episodes of respiratory infections, bronchial asthma, or gastroenteritis. Her sleep cycle was disorganized. Brain magnetic resonance imaging at 3 years of age demonstrated progressive atrophy of the cerebral hemisphere, cerebellum, and brainstem (Fig. 1c). EEG at 3 years showed borderline findings consisting of a predominance of fast wave activity with no spindle formation interrupted by slow wave burst. She recurrently suffered bone fractures without obvious event. Systemic bone X-ray at 12 years of age showed neurogenic arthrogryposis and osteoporosis. At 12 years of age, she was bedridden and was only able to roll over. She showed profound intellectual disability and had no meaningful words. Her epileptic seizures disappeared after 10 years of age, but epileptic discharges comprised of spike-and-slow wave complex at bilateral frontal area with low-amplitude irregular background activity were seen on EEG.

G-banded chromosomal analysis revealed a normal karyotype (46,XX). Metabolic screenings including amino acids, lactic acid, pyruvic acid, organic acids, lactic acid, and lysosomal enzymes were unremarkable. The biochemical analysis of blood repeatedly showed low levels of serum alkaline phosphatase from birth (186 U/l at birth and 326 U/l at 7 years of age [normal range, 450–1250 U/l]). Both concentrations of serum and urine calcium were normal (serum calcium, 9.6 mg/dl; U-calcium/U-creatinine ratio, 0.23 at 7 years of age).

DNA preparation

Peripheral blood samples were obtained from the patient and her parents after parents signed informed consent. DNA was extracted using QuickGene-610 L (Fujifilm, Tokyo, Japan) according to the manufacturer's instructions. The study was approved by the ethics committee of the Yokohama City University.

Whole exome sequencing

Patient DNA was captured with the SureSelect Human All Exon V5 Kit (Agilent Technologies, Santa Clara, CA, USA) and sequenced on an Illumina Hiseq2000 (Illumina, San Diego, CA, USA) with 101-bp paired-end reads. Image analysis and base calling were performed by sequence control software real-time analysis and CASAVA software v1.8 (Illumina). Reads were mapped to the human reference genome sequence (UCSC hg19, NCBI build 37) and aligned using Novoalign (Novocraft Technologies, Jaya, Malaysia). PCR duplicate reads were excluded using Picard (http://picard.sourceforge.net/) for further analysis. Single-nucleotide variants (SNVs) and small indels were identified using the Genome Analysis Toolkit UnifiedGenotyper [13] and filtered according to the Broad Institute's best-practice guidelines (version 3). Variants that passed the filters were annotated using ANNOVAR[14]. The damaging prediction was performed by Polyphen-2 [15] and MutationTaster software [16].

Sanger sequencing

PIGT exon 2 and exon 10 sequences were PCR amplified from the patient and her parents using the following primers: *PIGT* ex2F 5′-GGGAGGAACTTGTCATCACC-3′ and ex2R 5′-CAGTGGCAGGATGACAACAC-3′, *PIGT* ex10F 5′-AGAGATGTGGGTGACCTTGC-3′ and ex10R 5′-CTGAGGACAGATGGGCTACA-3′, respectively. Amplified PCR products were sequenced on an ABI 3500xl or 3130xl Genetic Analyzer (Applied Biosystems, Foster City, CA, USA).

Flow cytometry

Peripheral blood samples were collected from the patient and normal control individuals. Granulocyte surface expression of total GPI-APs was quantified by staining with Alexa 488-conjugated inactivated aerolysin (FLAER; Protox Biotech, Victoria, Canada). Expression of CD16, CD24, and alkaline phosphatase (ALP) was examined using appropriate primary antibodies (3G8, ML5, and B4-78, respectively; BD Biosciences, Franklin Lakes, NJ, USA), followed by a PE-conjugated anti-mouse IgG secondary antibody (BD Biosciences). Cells were analyzed by BD FACSCanto II (BD Biosciences).

Human *PIGT* cDNA (NM_015937.5) with FLAG at the C terminus was subcloned into the pME (driven by a strong SRα promoter) or pTA (driven by a weak promoter

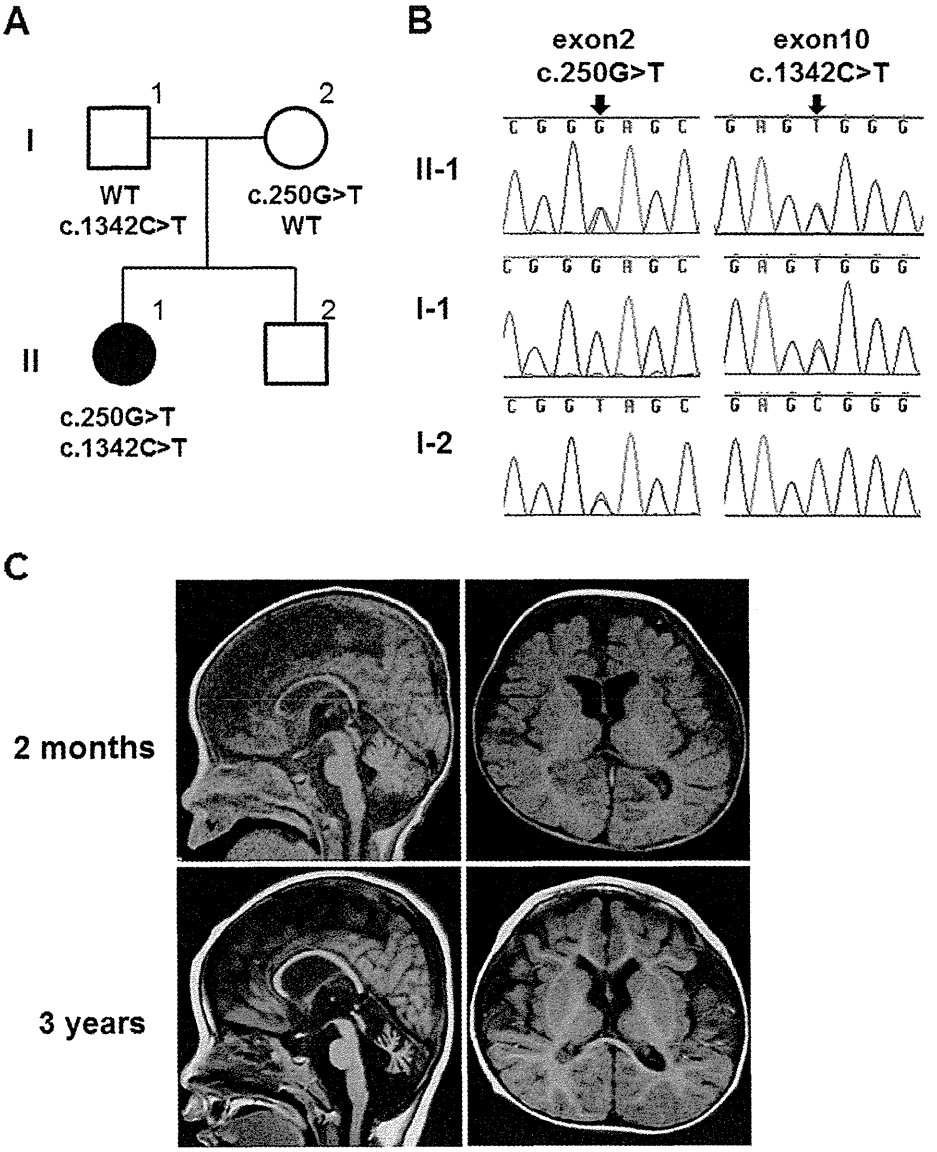

Fig. 1 **a** Familial pedigree. **b** Sanger sequencing results. Compound heterozygous mutations, c.250G>T and c.1342C>T, in *PIGT* were observed in the affected individual. c.250G>T (*left*) and c.1342C>T (*right*) were inherited from the mother and the father, respectively. **c** Magnetic resonance imaging of the patient's brain. Axial and sagittal T1-weighted images at 3 years of age show atrophic changes of the cerebral hemisphere, brainstem, and cerebellum

containing only TATA-box) vector [17]. Two *PIGT* mutants, Glu84* and Arg488Trp, were generated by site-directed mutagenesis. Mutant and wild-type *PIGT* plasmids were transfected by electroporation into CHO H4, *PIGT*-deficient Chinese hamster ovary (CHO) cells expressing human DAF (also called CD55) and CD59 as previously described [18]. Two days later, lysates were run on SDS-PAGE, and Western blotting was performed using an anti-FLAG antibody (M2; Sigma-Aldrich, St. Louis, MO, USA) to detect FLAG-tagged PIGT (PIGT-F). The protein levels were normalized to the loading control, and luciferase activities were used to evaluate transfection efficiencies. Cells were stained with anti-hCD59 (5H8), anti-hDAF (IA10), and anti-Hamster uPAR (5D6) antibodies and restoration of the surface expression of GPI-APs was assessed by flow cytometry.

Results

Mutation screening

We performed mutation screening for previously reported genes involved in the GPI-anchor–synthesis pathway, and identified the compound heterozygous mutations c.250G>T (p. Glu84*) and c.1342C>T (p. Arg488Trp) in *PIGT* (NM_015937.5). Both mutations were not found in 6500

ESP (Exome Sequencing Project) or 1000 genomes [19, 20], but c.1342C>T is present in one of 408 in-house control exomes. Both mutations were predicted to be probably disease-causing by Polyphen-2 and MutationTaster. Sanger sequencing confirmed that c.250G>T and c.1342C>T were inherited from the mother and father, respectively (Fig. 1b).

Functional effect of the mutations on GPI synthesis

PIGT is a component of GPI transamidase that mediates the post-translational attachment of GPI anchors to the C-terminal of the precursor protein. Therefore, the mutant GPI transamidase is likely to impair the surface expression of GPI-APs. To investigate the influence of *PIGT* mutations on GPI-APs synthesis, we first examined the granulocyte surface expression of GPI-APs from the patient and a healthy control. Expression of total GPI-APs (FLAER staining) and GPI-APs CD16 and ALP on granulocytes was reduced in the patient compared to the normal control (Fig. 2a). However, similar expression levels of another GPI-AP CD24 were seen in the patient and control (Fig. 2a).

We then transiently transfected wild-type or mutant (Glu84* or Arg488Trp) *PIGT* cDNA constructs into *PIGT*-deficient CHO cells to evaluate the functional effect of each mutation on GPI-AP expression. Western blotting revealed that the expression level of Arg488Trp mutant protein was similar to that of wild-type protein, whereas the Glu84* mutant expressed a small amount of full-length protein (probably read-though) (Fig. 2c). Wild-type *PIGT* transfection successfully restored the expression of GPI-APs CD59, DAF (CD55), and uPAR in both cases using vectors with a strong (pME) and weak (pTA) promoter (Fig. 2b). The Arg488Trp mutant *PIGT* cloned in pME restored the expression of GPI-APs close to that of wild-type, whereas the same mutant in the pTA vector only partially restored expression. The Glu84* mutant *PIGT* in the pME vector insufficiently restored the expression of GPI-APs, while this mutant in the pTA vector could not restore expression (Fig. 2b). These results demonstrate that both mutants, especially the Glu84* alteration, reduce the activity of PIGT function.

Fig. 2 **a** Surface expression of GPI-APs on granulocytes. Granulocytes from the patient and healthy control were stained with FLAER or antibodies against CD24, CD16, and ALP. The expression of total GPI, CD16, and ALP in the patient (*solid line*) was lower than in the normal control (*dark shaded area*). CD24 expression did not differ between the patient and control. The *light shaded areas* represent the isotype control. *X* axes show fluorescent intensities, which indicate expression levels of each GPI-AP on the cell surface. *Y* axes show the relative cell numbers. The value of mean fluorescent intensities of each sample is shown in each panel. **b** PIGT-deficient CHO cells were transiently transfected with wild-type (*dashed line*), Glu84* mutant (*fine solid line*), or Arg488Trp mutant (*bold solid line*) *PIGT* cDNA expression constructs in vectors with either a strong promoter (pME; *upper panels*) or weak promoter (pTA; *lower panels*). PIGT-F protein levels and restoration of the surface expression of CD59, DAF, and uPAR were assessed 2 days later. The *dark* and *light shadows* represent empty-vector transfectants and isotype controls, respectively. **c** Western blotting showed that the Arg488Trp mutant protein was expressed at similar levels to the wild-type protein, whereas the Glu84* mutant full-length protein, representing the read-through product, was expressed at lower levels. Quantity numbers at the bottom of the gel indicate the relative intensity of PIGT-F protein levels normalized to the loading control, and luciferase activities used for evaluating transfection efficiencies. *Arrowhead* indicates a non-specific product

Discussion

GPI deficiency syndromes are recessive disorders caused by mutations in genes involved in the GPI-anchor biosynthesis pathway. Here, we describe novel compound heterozygous *PIGT* mutations in a nonconsanguineous patient presenting with seizures and intellectual disability.

The first reported *PIGT* mutation (c.547A>C, p.Thr183Pro) was identified in a consanguineous Turkish family who showed seizures, intellectual disability, and multiple congenital anomalies [12]. A decreased expression of GPI-APs was documented on patient granulocytes. They confirmed that the homozygous c.547A>C mutation impaired the function of PIGT by the functional study using *pigt* knockdown zebrafish embryos which showed gastrulation defects phenotype. In the present study, we also demonstrated that both *PIGT* mutations, c.250G>T (p. Glu84*) and c.1342C>T (p. Arg488Trp), impaired the function of PIGT which was confirmed by the functional study using the PIGT deficient CHO cells.

Mammalian GPI transamidase consists of at least five subunits, PIGK, GPAA1, PIGS, PIGT, and PIGU [1]. Of these, PIGT plays a critical role in stabilizing the complex formation of GPI transamidase [17], which mediates cleavage of the GPI attachment signal peptide at the C-terminal of the precursor protein and transfers GPI anchors to the C-terminal of cleaved proteins [1]. Consequently, PIGT mutants may not be able to correctly form the GPI transamidase complex, leading to a loss of GPI transamidase activity and reduction in the cellular surface expression of GPI-APs.

Our patient and four patients described by Kvarnung et al. [12] showed broad clinical spectrum and shared several common features (Table 1). The neurological findings including intractable seizures, hypotonia and severe intellectual disability were observed in all patients. Ophthalmologic features including strabismus, nystagmus, and cerebral visual impairment were also observed in all. Cerebral and cerebellar atrophy was observed in our patient and two of four seen by Kvarnung et al. The EEG findings in our patient were also exacerbated as she grew, suggesting progressive encephalopathy. Our patient and three of four patients by Kvarnung et al. had some cardiologic disorders. All patients had some

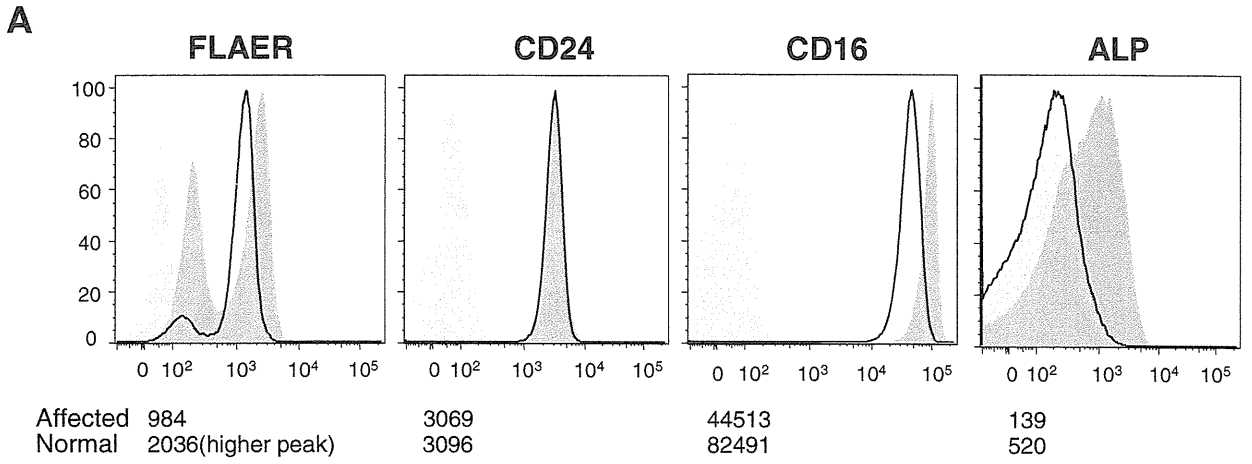
A
FLAER
CD24
CD16
ALP
Affected 984 3069 44513 139
Normal 2036(higher peak) 3096 82491 520

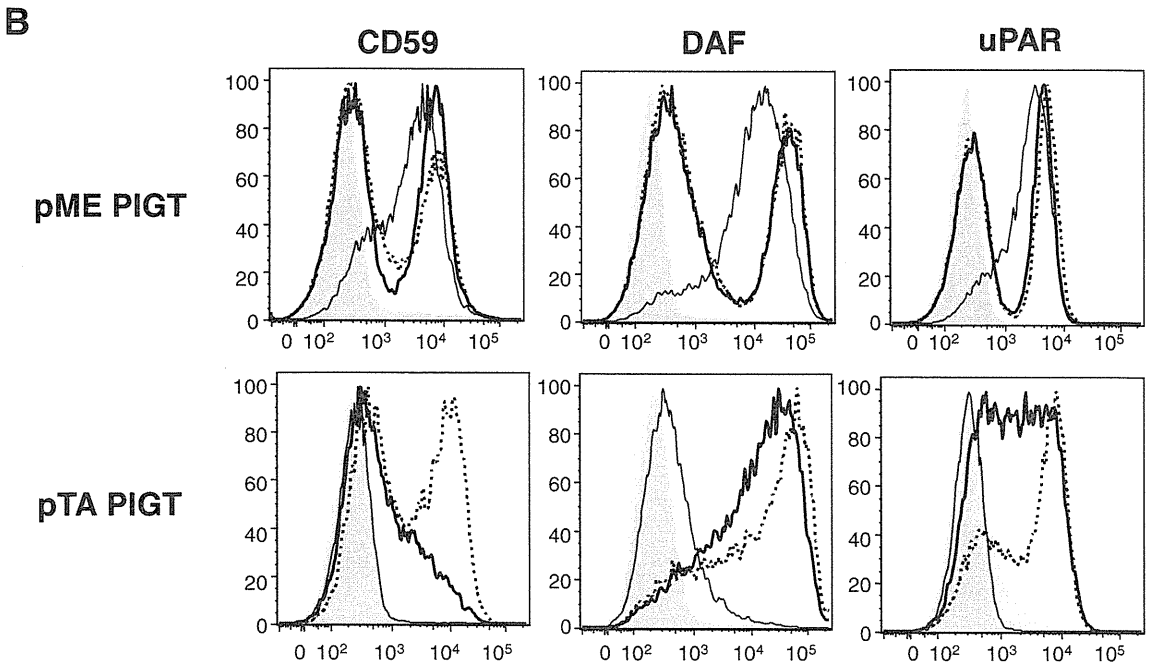
B
CD59
DAF
uPAR
pME PIGT
pTA PIGT

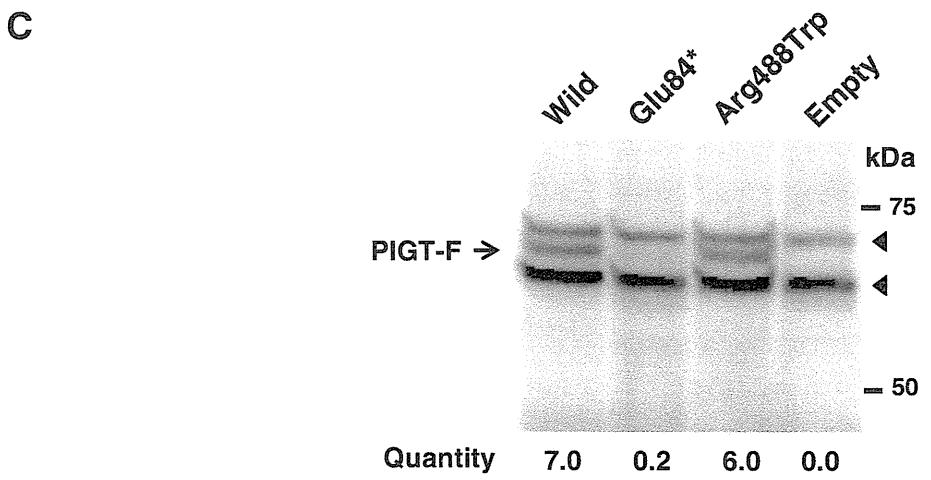
C
Wild
Glu84*
Arg488Trp
Empty
kDa
75
50
PIGT-F
Quantity 7.0 0.2 6.0 0.0

Table 1 Clinical features of patients with PIGT mutations

Patients	This Patient	Kvarnung et al. Patient 1	Kvarnung et al. Patient 2	Kvarnung et al. Patient 3	Kvarnung et al. Patient 4
consanguinity	–	+	+	+	+
Sex	Female	Female	Female	Female	Female
Gestation	40 weeks	40 weeks	39 weeks	37 weeks	37 weeks
Birth weight	3,816 g	4,735 g	4,500 g	3,460 g	3,240 g
Birth length	51 cm	53 cm	54 cm	53 cm	53 cm
BHC	35.5 cm +1.8 SD	38 cm +2 SD	39 cm +3 SD	35 cm +1 SD	36 cm +1.5 SD
HPP	+	+	+	+	+
ID	+	+	+	+	+
Hypotonia	+	+	+	+	+
Seizure	+	+	+	+	+
Strabismus	+	+	+	+	+
Nystagmus	+	+	+	+	+
CVI	+	+	+	+	+
Brain images	CT: dilated ventricle, frontal atrophy, cerebellar and brainstem atrophy	CT: primitive Sylvian fissures	CT: Normal findings	MRI: global atrophy with predominate vermis and cerebellar atrophy, atrophy of basal ganglia	MRI: global atrophy with predominat vermis and cerebellar atrophy, hypomyelination
Tooth abnormalities	–	+	+	+	+
Skeletal features	Scoliosis, osteoporosis	Craniosynostosis, Pectus excavatum, Short arm, Scoliosis, Delayed bone age, Reduced mineralisation	Craniosynostosis, short arm, Scoliosis, Delayed bone age, Reduced mineralisation	Short arm, Delayed bone age, Reduced mineralisation	Short arm, Delayed bone age, Reduced mineralisation
Urologic features	Urolithiasis, Ureteral dilation	Nephrocalcinosis	Nephrocalcinosis, Ureteral dilation, Cysts and dysplasia	Nephrocalcinosis, Ureteral dilation	Nephrocalcinosis, Ureteral dilation
Cardiologic features	PDA	Minor PDA	–	Mild restrictive CMP	Increased atrial load on ECG
Facial features	Low set ears, micrognathia, malar flattening, upslanting palpebral fissures, depressed nasal bridge, short anteverted nose, downturned corners of the mouth, tented lip, high arched palate	High forehead with bitemporal narrowing, broad nasal root, anteverted nose, long philtrum with a deep groove, distinct cupid bow	High forehead with bitemporal narrowing, broad nasal root, anteverted nose, long philtrum with a deep groove, distinct cupid bow	High forehead with bitemporal narrowing, broad nasal root, anteverted nose, long philtrum with a deep groove, distinct cupid bow	High forehead with bitemporal narrowing, broad nasal root, anteverted nose, long philtrum with a deep groove, distinct cupid bow

BHC birth head circumference, *HPP* hypophosphatasia, *ID* intellectual disability, *CVI* cerebral visual impairment, *ECG* electrocardiogram, *CMP* cardiomyopathy, *PDA* patent ductus arteriosus

urologic features, but not nephrocalcinosis in our patient. Our case shared similar facial features with previous patients including a depressed nasal bridge, short anteverted nose, tented lip, and downturned corners of the mouth. Low set ears, micrognathia, malar flattening, and upslanting palpebral fissures were unique to our patient.

Hyperphosphatasia is a characteristic symptom of some GPI deficiencies, such as PIGV, PIGW, PIGO, PGAP2 and PGAP3 deficiencies [2–6]. In contrast, hypophosphatasia is a particularly distinctive feature in the loss of GPI transamidase function. Murakami at al. suggested that GPI transamidase abnormalities lead to an inability to hydrolyze the precursor protein of alkaline phosphatase, resulting in the degradation of most precursor proteins within the cell and a decrease of serum alkaline phosphatase levels (hypophosphatasia) [21]. This is supported in our case by the hypophosphatasia. The patients described by Kvarnung et al. showed hypercalcemia and hypercalciuria following tooth abnormality, craniosynostosis, a delayed bone age, and reduced mineralization, which is the common features with infantile hypophosphatasia caused by the mutations in *ALPL*, the gene encoding tissue non-specific alkaline phosphatase (TNAP) [22]. As TNAP is a GPI-AP, the PIGT deficiency causes decreased surface expression of TNAP, which would lead to bone abnormalities. Regardless of hypophosphatasia, our case showed only mild scoliosis and osteoporosis, but no tooth abnormality nor craniosynostosis. Different mutational effects on the enzyme activity may account for such different phenotypes. In this study, mutant PIGT construct harboring Arg488Trp or Glu84* in strong promoter (pME) vector restored GPI-Aps expression. In contrast, Kvarnung et al. showed that abnormal phenotype of pigt knockdown zebrafish was never restored by the homozygous mutant (Thr183Pro) PIGT cDNA. Therefore, it is possible to estimate that the Thr183Pro mutation may affect the GPI transamidase complex activity more severely than the Arg488Trp and Glu84* mutations, leading to less severe phenotypes. However, further functional analysis and cases with *PIGT* mutations are needed to elucidate the relevance of these mutations in PIGT function and full clinical spectrum of GPI deficiency syndromes.

Acknowledgments We thank the patient's family for participating in this work. We also thank Nobuko Watanabe for her technical assistance. This study was supported by the Ministry of Health, Labour and Welfare of Japan, a Grant-in-Aid for Scientific Research (A), (B), and (C) from the Japan Society for the Promotion of Science, the Takeda Science Foundation, the fund for Creation of Innovation Centers for Advanced Interdisciplinary Research Areas Program in the Project for Developing Innovation Systems, the Strategic Research Program for Brain Sciences, and a Grant-in-Aid for Scientific Research on Innovative Areas (Transcription Cycle) from the Ministry of Education, Culture, Sports, Science and Technology of Japan.

Conflict of interest The authors declare that they have no conflict of interest.

References

1. Kinoshita T, Fujita M, Maeda Y (2008) Biosynthesis, remodelling and functions of mammalian GPI-anchored proteins: recent progress. J Biochem 144(3):287–294. doi:10.1093/jb/mvn090
2. Krawitz PM, Schweiger MR, Rodelsperger C, Marcelis C, Kolsch U, Meisel C, Stephani F, Kinoshita T, Murakami Y, Bauer S, Isau M, Fischer A, Dahl A, Kerick M, Hecht J, Kohler S, Jager M, Grunhagen J, de Condor BJ, Doelken S, Brunner HG, Meinecke P, Passarge E, Thompson MD, Cole DE, Horn D, Roscioli T, Mundlos S, Robinson PN (2010) Identity-by-descent filtering of exome sequence data identifies PIGV mutations in hyperphosphatasia mental retardation syndrome. Nat Genet 42(10):827–829. doi:10.1038/ng.653
3. Krawitz PM, Murakami Y, Hecht J, Kruger U, Holder SE, Mortier GR, Delle Chiaie B, De Baere E, Thompson MD, Roscioli T, Kielbasa S, Kinoshita T, Mundlos S, Robinson PN, Horn D (2012) Mutations in PIGO, a member of the GPI-anchor-synthesis pathway, cause hyperphosphatasia with mental retardation. Am J Hum Genet 91(1):146–151. doi:10.1016/j.ajhg.2012.05.004
4. Hansen L, Tawamie H, Murakami Y, Mang Y, ur Rehman S, Buchert R, Schaffer S, Muhammad S, Bak M, Nothen MM, Bennett EP, Maeda Y, Aigner M, Reis A, Kinoshita T, Tommerup N, Baig SM, Abou Jamra R (2013) Hypomorphic mutations in PGAP2, encoding a GPI-anchor-remodeling protein, cause autosomal-recessive intellectual disability. Am J Hum Genet 92(4):575–583. doi:10.1016/j.ajhg.2013.03.008
5. Howard MF, Murakami Y, Pagnamenta AT, Daumer-Haas C, Fischer B, Hecht J, Keays DA, Knight SJ, Kolsch U, Kruger U, Leiz S, Maeda Y, Mitchell D, Mundlos S, Phillips JA 3rd, Robinson PN, Kini U, Taylor JC, Horn D, Kinoshita T, Krawitz PM (2014) Mutations in PGAP3 impair GPI-anchor maturation, causing a subtype of hyperphosphatasia with mental retardation. Am J Hum Genet 94(2):278–287. doi:10.1016/j.ajhg.2013.12.012
6. Chiyonobu T, Inoue N, Morimoto M, Kinoshita T, Murakami Y (2013) Glycosylphosphatidylinositol (GPI) anchor deficiency caused by mutations in PIGW is associated with West syndrome and hyperphosphatasia with mental retardation syndrome. J Med Genet. doi:10.1136/jmedgenet-2013-102156
7. Krawitz PM, Murakami Y, Riess A, Hietala M, Kruger U, Zhu N, Kinoshita T, Mundlos S, Hecht J, Robinson PN, Horn D (2013) PGAP2 mutations, affecting the GPI-anchor-synthesis pathway, cause hyperphosphatasia with mental retardation syndrome. Am J Hum Genet 92(4):584–589. doi:10.1016/j.ajhg.2013.03.011
8. Almeida AM, Murakami Y, Layton DM, Hillmen P, Sellick GS, Maeda Y, Richards S, Patterson S, Kotsianidis I, Mollica L, Crawford DH, Baker A, Ferguson M, Roberts I, Houlston R, Kinoshita T, Karadimitris A (2006) Hypomorphic promoter mutation in PIGM causes inherited glycosylphosphatidylinositol deficiency. Nat Med 12(7):846–851. doi:10.1038/nm1410
9. Ng BG, Hackmann K, Jones MA, Eroshkin AM, He P, Wiliams R, Bhide S, Cantagrel V, Gleeson JG, Paller AS, Schnur RE, Tinschert S, Zunich J, Hegde MR, Freeze HH (2012) Mutations in the glycosylphosphatidylinositol gene PIGL cause CHIME syndrome. Am J Hum Genet 90(4):685–688. doi:10.1016/j.ajhg.2012.02.010
10. Johnston JJ, Gropman AL, Sapp JC, Teer JK, Martin JM, Liu CF, Yuan X, Ye Z, Cheng L, Brodsky RA, Biesecker LG (2012) The phenotype of a germline mutation in PIGA: the gene somatically mutated in paroxysmal nocturnal hemoglobinuria. Am J Hum Genet 90(2):295–300. doi:10.1016/j.ajhg.2011.11.031
11. Krawitz PM, Hochsmann B, Murakami Y, Teubner B, Kruger U, Klopocki E, Neitzel H, Hoellein A, Schneider C, Parkhomchuk D, Hecht J, Robinson PN, Mundlos S, Kinoshita T, Schrezenmeier H (2013) A case of paroxysmal nocturnal hemoglobinuria caused by a

germline mutation and a somatic mutation in PIGT. Blood 122(7): 1312–1315. doi:10.1182/blood-2013-01-481499
12. Kvarnung M, Nilsson D, Lindstrand A, Korenke GC, Chiang SC, Blennow E, Bergmann M, Stodberg T, Makitie O, Anderlid BM, Bryceson YT, Nordenskjold M, Nordgren A (2013) A novel intellectual disability syndrome caused by GPI anchor deficiency due to homozygous mutations in PIGT. J Med Genet 50(8):521–528. doi: 10.1136/jmedgenet-2013-101654
13. DePristo MA, Banks E, Poplin R, Garimella KV, Maguire JR, Hartl C, Philippakis AA, del Angel G, Rivas MA, Hanna M, McKenna A, Fennell TJ, Kernytsky AM, Sivachenko AY, Cibulskis K, Gabriel SB, Altshuler D, Daly MJ (2011) A framework for variation discovery and genotyping using next-generation DNA sequencing data. Nat Genet 43(5):491–498. doi:10.1038/ng.806
14. Wang K, Li M, Hakonarson H (2010) ANNOVAR: functional annotation of genetic variants from high-throughput sequencing data. Nucleic Acids Res 38(16):e164. doi:10.1093/nar/gkq603
15. Adzhubei IA, Schmidt S, Peshkin L, Ramensky VE, Gerasimova A, Bork P, Kondrashov AS, Sunyaev SR (2010) A method and server for predicting damaging missense mutations. Nat Methods 7(4):248–249. doi:10.1038/nmeth0410-248
16. Schwarz JM, Rodelsperger C, Schuelke M, Seelow D (2010) MutationTaster evaluates disease-causing potential of sequence alterations. Nat Methods 7(8):575–576. doi:10.1038/nmeth0810-575
17. Ohishi K, Inoue N, Kinoshita T (2001) PIG-S and PIG-T, essential for GPI anchor attachment to proteins, form a complex with GAA1 and GPI8. EMBO J 20(15):4088–4098. doi:10.1093/emboj/20.15.4088
18. Ashida H, Hong Y, Murakami Y, Shishioh N, Sugimoto N, Kim YU, Maeda Y, Kinoshita T (2005) Mammalian PIG-X and yeast Pbn1p are the essential components of glycosylphosphatidylinositol-mannosyltransferase I. Mol Biol Cell 16(3):1439–1448. doi:10.1091/mbc.E04-09-0802
19. Genomes Project C, Abecasis GR, Altshuler D, Auton A, Brooks LD, Durbin RM, Gibbs RA, Hurles ME, McVean GA (2010) A map of human genome variation from population-scale sequencing. Nature 467(7319):1061–1073. doi:10.1038/nature09534
20. Genomes Project C, Abecasis GR, Auton A, Brooks LD, DePristo MA, Durbin RM, Handsaker RE, Kang HM, Marth GT, McVean GA (2012) An integrated map of genetic variation from 1,092 human genomes. Nature 491(7422):56–65. doi:10.1038/nature11632
21. Murakami Y, Kanzawa N, Saito K, Krawitz PM, Mundlos S, Robinson PN, Karadimitris A, Maeda Y, Kinoshita T (2012) Mechanism for release of alkaline phosphatase caused by glycosylphosphatidylinositol deficiency in patients with hyperphosphatasia mental retardation syndrome. J Biol Chem 287(9):6318–6325. doi:10.1074/jbc.M111.331090
22. Mornet E (2007) Hypophosphatasia. Orphanet J Rare Dis 2:40. doi: 10.1186/1750-1172-2-40